Energy Engineering

Tech Science Press

Doi:10.32604/ee.2025.064160

ARTICLE

Impact of Short-Term Power Shortage from Low Voltage Ride through and DC Commutation Failure on Power Grid Frequency Stability

Wenjia Zhang*, Sixuan Xu, Wanchun Qi, Zhuyi Peng and Wentao Sun

Institute of Economics and Technology, State Grid Jiangsu Electric Power Co., Ltd., Nanjing, 610095, China

*Corresponding Author: Wenjia Zhang. Email: zhangwenjiapd@163.com

Received: 07 February 2025; Accepted: 25 April 2025; Published: 29 May 2025

ABSTRACT: Countries worldwide are advocating for energy transition initiatives to promote the construction of low-carbon energy systems. The low voltage ride through (LVRT) characteristics of renewable energy units and commutation failures in line commutated converter high voltage direct current (LCC-HVDC) systems at the receiving end leads to short-term power shortage (STPS), which differs from traditional frequency stability issues. STPS occurs during the generator's power angle swing phase, before the governor responds, and is on a timescale that is not related to primary frequency regulation. This paper addresses these challenges by examining the impact of LVRT on voltage stability, developing a frequency response model to analyze the mechanism of frequency instability caused by STPS, deriving the impact of STPS on the maximum frequency deviation, and introducing an energy deficiency factor to assess its impact on regional frequency stability. The East China Power Grid is used as a case study, where the energy deficiency factor is calculated to validate the proposed mechanism. STPS is mainly compensated by the rotor kinetic energy of the generators in this region, with minimal impact on other regions. It is concluded that the energy deficiency factor provides an effective explanation for the spatial distribution of the impact of STPS on system frequency.

KEYWORDS: Commutation failure; frequency stability; LVRT; renewable energy; short-term power shortage; LCC-HVDC

1 Introduction

As global energy shortages, resource constraints, and environmental pollution intensify, countries are advocating for energy transition initiatives to promote the construction of low-carbon energy systems [1]. High penetration of renewable energy and a high proportion of power electronic devices are the main features of this new system. For the receiving grid, there are two major changes. On one hand, the installation capacity and power generation capacity of renewable energy in the receiving grid are increasing. On the other hand, large-scale renewable energy bases, such as wind and photovoltaic (PV) farms, feed external renewable energy into the receiving grid through HVDC transmission. These two factors contribute to the gradual increase in the penetration of renewable energy in the receiving grid [2]. In terms of grid connection methods, renewable energy can be integrated through both AC and DC grids. In the event of a short-circuit fault at the grid connection bus, renewable energy units may enter LVRT mode [3], and HVDC transmission may experience commutation failure [4], which could lead to an STPS in the power system. As renewable energy penetration increases, STPS are more likely to become a factor influencing the frequency stability of the power system in the near future. Therefore, it is necessary to study the mechanisms and evaluation methods of frequency instability caused by STPS.

Research on the frequency characteristics and control measures of traditional grids is already quite mature. The average system frequency (ASF) model is the most classic and widely applied method in the equivalent model approach [5]. Egido et al. [6] simplify the governor system in the ASF model to a first-order system, resulting in the first-order average system frequency (FASF) model. This simplification makes the model solution more convenient and faster. To investigate the impact of STPS on system frequency stability constraints, O' Sullivan et al. [7] studied the maximum penetration of asynchronous generation in a European grid and found that wind power LVRT due to grid faults could have a more severe impact on frequency than large unit tripping. If low frequency triggers ROCOF (rate of change of frequency) protection, it could worsen the situation. The study suggested disabling ROCOF protection and enabling wind power inertia as countermeasures. Wang and Strbac [8] present an optimization model that integrates transient stability constraints, introducing a novel Transient Stability-Constrained Optimal Power Flow (TSC-OPF) approach. However, similar to other optimization methods, it lacks an explicit explanation of the underlying causes of system stability or instability, as the optimization process functions as a "black box." Yan et al. [9] propose an innovative approach to modeling and controlling load frequency in multi-region power systems using multiple first-order dynamic fractional-order Type-2 Fuzzy Logic Systems (T2-FLSs). It emphasizes the design of the controller; however, similar to the previous work discussed, it does not address the issue of frequency stability caused by STPS. According to Dai et al. [10], to overcome the limitations of conventional methods, different operational regions of wind turbine generators (WTGs) and wind speed disturbances are fully taken into account, and a frequency response model of wind power (WPFR) participating in primary frequency control is developed using small signal analysis theory. Qazi et al. [11] investigate the impacts of fault ride-through behavior of wind farms on system stability in detail, using a full dynamic model of a low-inertia island power system. Njoka et al. [12] analyze the impact of renewable energy penetration on system frequency, noting that at high penetration levels, frequency instability occurs, but lack a quantitative analysis of the instability mechanism. The shape and mechanism of voltage-frequency coupled transient instability during LVRT are investigated in detail using the voltage-vector-triangle graphic (VTG) method in Pei et al. [13]. Choopani et al. [14] examine a novel method for improving the transient stability of multi-virtual synchronous generator (VSG) grids, aiming to control the oscillation of VSGs relative to the center of inertia frequency (COI-frequency) of the grid during short-circuit events.

However, existing studies have not fully clarified the fundamental differences between STPS and permanent faults on system frequency. While both types of disturbances can affect the grid's frequency stability, their underlying mechanisms and the duration of their impacts differ significantly. Furthermore, the spatial distribution of the impact of STPS on system frequency has not been deeply analyzed. Understanding how STPS caused by renewable energy fluctuations, LVRT, or HVDC commutation failures propagate through different regions of the power grid is crucial. These differences may lead to region-specific frequency responses and necessitate more targeted control strategies for maintaining grid stability.

To address these issues, this paper analyzes the impact of STPS on power grid frequency stability.

The main contributions of this paper are:

(1) Introduction of LVRT Characteristics: The paper introduces the LVRT characteristics of renewable energy units and analyzes the impact of LVRT on voltage stability.
(2) Frequency Response Model: A frequency response model is established to analyze the mechanism of frequency instability caused by STPS.
(3) Energy Deficiency Factor: A novel energy deficiency factor is proposed to evaluate the impact of STPS on regional frequency stability.
(4) Case Study on East China Power Grid: The East China Power Grid is used as a case study to calculate the energy deficiency factor and verify the proposed mechanism of frequency instability caused by STPS.

The conclusion is drawn that the energy deficiency factor can effectively explain the spatial distribution of the impact of STPS on system frequency.

2 LVRT Characteristics of Renewable Energy Units and Their Impact on Voltage Stability

For renewable energy units and DC systems, a short-term power loss on the order of hundreds of milliseconds occurs during AC voltage sags. For renewable energy units, an AC voltage drop triggers the LVRT strategy. During LVRT, the renewable energy unit reduces its active current. For DC systems, an AC voltage drop leads to commutation failure, during which the active power of the DC system is approximately zero [15]. There is extensive literature on DC commutation failure. The following presents the current LVRT strategy settings for renewable energy units.

2.1 LVRT Characteristics of Renewable Energy Units and Their Impact on Voltage Stability

In China, the existing LVRT characteristics and parameter settings for wind and PV units typically have the following features:

(1) LVRT strategy is activated when the unit output voltage drops below 0.9 pu and is deactivated when the output voltage rises above 0.9 pu.

(2) According to the reference [16], during symmetrical faults, the dynamic reactive current increment of the wind farm should respond to the voltage changes at the grid connection point, and it must satisfy the following equation:

$$\Delta I_t = K_1 \times (0.9 - U_t) \times I_N, 0.2 \le U_t \le 0.9, \tag{1}$$

where ΔI_t is the dynamic reactive current increment injected by the wind farm, K_1 is the dynamic reactive current coefficient of the wind farm (typically in the range of [1.5, 3]), U_t is the voltage at the wind farm grid connection point in per unit, and I_N is the rated current of the wind farm.

(3) During LVRT, the active power control method is based on a specified percentage of current control. If active power priority is given, this percentage can be set to 100%. Under reactive power priority conditions, it can be set to a lower value or even 0.

(4) After the fault, active power can be restored either at a certain rate or immediately.

2.2 Impact on Voltage Stability

To analyze the key factors influencing voltage stability control, a dual-machine single-load system model, as shown in Fig. 1 [17], is established. The power side of the system includes a synchronous generator and a wind-PV unit based on an inverter, both of which supply power to a common load. There are impedances between the synchronous generator and the wind-PV unit, as well as between the wind-PV unit and the load.

In Fig. 1, E_{sys} and θ_{sys} represent the terminal voltage amplitude and phase of the synchronous generator, respectively. P_{sys} and Q_{sys} are the active and reactive power outputs of the synchronous generator, respectively. X_{sys} is the reactance between the synchronous generator and the wind-PV unit. U_n and θ_n are the voltage amplitude and phase at the grid connection point of the wind-PV unit, respectively, while P_n and Q_n are the active and reactive power outputs of the wind-PV unit, respectively. X_n represents the reactance between the grid connection point of the wind-PV unit and the load node. U_L and θ_L are the voltage amplitude and phase at the load node, and P_L and Q_L are the active and reactive power of the load, respectively.

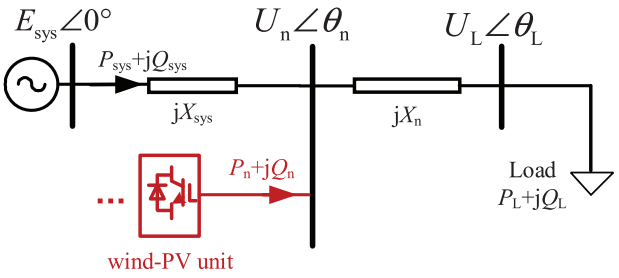

Figure 1: Dual-machine single-load system model

In power systems dominated by synchronous generators, thanks to the magnetic field energy in the stator windings, synchronous generators can typically respond in real time to both active and reactive power demands of the load. Therefore, in the analysis of key factors affecting voltage stability in traditional power systems, the focus is usually on adjusting the system' s equivalent impedance and load power. However, in power systems with a high proportion of asynchronous generators (e.g., wind and PV units), the output power magnitude and power factor of the asynchronous sources have a significant impact on the system's power flow distribution and the voltage at load nodes. The following discussion primarily focuses on the influence of asynchronous generator output variations and their LVRT parameters on system voltage stability.

To study the impact of wind and PV unit output characteristics on system voltage stability, the parameters of the system shown in Fig. 1 for the dual-machine single-load system are selected as shown in Table 1.

Table 1: Dual-machine single-load system parameters

Parameter	Value
Electromotive force of the synchronous generator E_{sys}/pu	1.1
Line reactance X_{sys}/pu	0.14
Line reactance X_n/pu	0.06
Active power of the load P_L/pu	1.2
Power factor of the load	0.9
Active power of the wind-PV power generation unit P_L/pu	0.4
Power factor of the wind-PV power generation unit	1.0

Based on the above parameters, the change in the load node voltage magnitude with respect to the power factor of the wind-PV unit is shown in Fig. 2a. From Fig. 2a, it can be seen that as the power factor of the wind-PV unit increases from 0 to 1, the load bus voltage initially increases slightly and then begins to decrease as the power factor continues to rise. When the power factor of the wind-PV unit is 0, the wind-PV unit only outputs reactive power, and the voltage drop across the reactance X_{sys} mainly results from the active power transmission along the line. Therefore, when the wind-PV unit increases its active power output, partially compensating for the active load, the load node voltage magnitude increases slightly. However, overall, the load node voltage magnitude decreases as the power factor of the wind-PV unit increases. This indicates that, under the condition of fixed apparent power, increasing the output of reactive power from the wind-PV unit is more beneficial to the system's voltage stability.

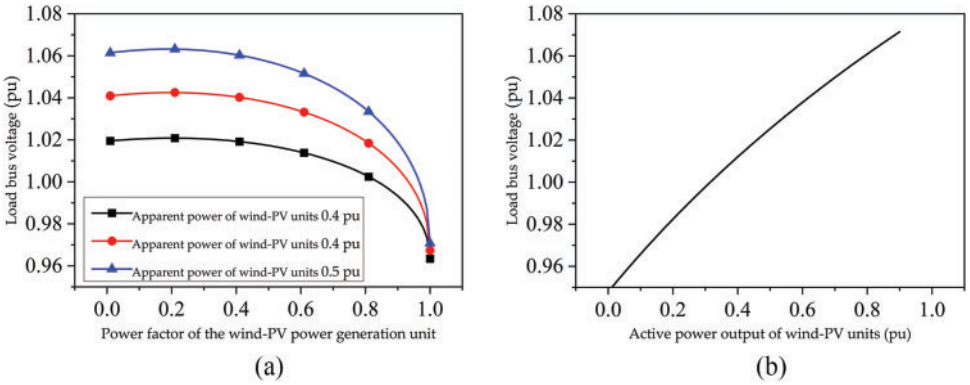

Figure 2: The impact of wind-PV on voltage. **(a)** The variation of the load bus voltage with the power factor of the wind-PV power generation unit; **(b)** The variation of the load bus voltage with the output active power of the wind-solar power generation unit

Next, examine the impact of the wind-PV unit's output power magnitude on system voltage stability. By fixing the power factor of the wind-PV unit and varying its output power, the change in load bus voltage magnitude with respect to the output power of the unit is shown in Fig. 2b.

From Fig. 2b, it can be observed that as the output power of the wind-PV unit increases, the load bus voltage magnitude increases monotonically.

Based on the above analysis, the following conclusions can be drawn:

During LVRT, the larger the output power of the wind-PV unit, the more beneficial it is for system voltage stability. For a fixed apparent power, the greater the reactive power output of the wind-PV unit, the more beneficial it is for system voltage stability. To improve system voltage stability, the wind-PV unit should adopt a reactive current priority LVRT strategy and maximize its output power as much as possible.

2.3 The Coupling Relationship between Active and Reactive Power

As mentioned above, after wind turbines and PV enter LVRT, a reactive power-priority control strategy is often adopted to ensure voltage stability. In this case, a shortage of active power may occur, which can impact the system frequency. To reduce the active power surge, the active current is also controlled during LVRT, and the specific control method is given by Eq. (2).

$$\begin{cases} i_{\mathrm{d}}{}^{*} = \min\left(i_{\mathrm{d0}}, \sqrt{I_{\max}{}^{2} - i_{\mathrm{q}}{}^{*2}}\right) \\ i_{\mathrm{q}}{}^{*} = K_1 \times (0.9 - U_{\mathrm{t}}) \times I_{\mathrm{N}}, 0.2 \le U_{\mathrm{t}} \le 0.9, \end{cases} \tag{2}$$

where $I_{\max}$ is the current limit of the inverter, $i_{\mathrm{d0}}{}^{*}$ is the reference value of the active under steady-state operating conditions, $I_{\mathrm{d}}{}^{*}$ and $I_{\mathrm{q}}{}^{*}$ are the reference values of the active and reactive current, respectively.

Due to the current limitation of the inverter, in order to minimize the active power impact as much as possible, the active current in Eq. (2) is taken as the minimum value between the pre-fault active current and the remaining capacity. It can be seen that when the voltage drop is deep, the reactive current is prioritized, and the active current cannot be maintained at its pre-fault level. Conversely, when the voltage drop is shallow, the active current can be maintained at its pre-fault level. Therefore, during LVRT, there is a strong coupling relationship between active and reactive power. The impact of reactive power on voltage stability has been analyzed previously. The following section will analyze the short-term active power shortage caused by LVRT and its impact on the system frequency.

3 The Impact of Short-Term Power Shortages on Frequency Stability

3.1. *Analysis of Maximum Frequency Deviation*

In a power grid with renewable energy units, its primary frequency control model can be equivalently represented by the simple model shown in Fig. 3 [18,19]. In this model, it is assumed that the frequency across the entire grid is uniform and that all thermal power plants are homogenous. As a result, the primary frequency control effects of all hydroelectric units in the system are equivalently modeled as a single turbine with a series droop coefficient. The role of wind and PV units in primary frequency control is typically categorized into two types: inertia support and damping support. Therefore, the primary frequency control characteristics of a grid with renewable energy units can be represented by the simplified model shown in Fig. 3.

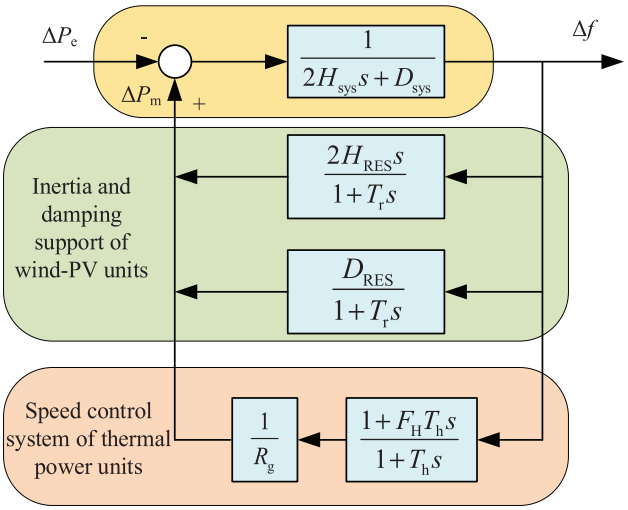

Figure 3: Primary frequency regulation simplified model

In the Fig. 3, H_{sys} and D_{sys} are the system equivalent inertia and damping coefficients, H_{RES} and D_{RES} are the support inertia and damping magnitude provided by the wind turbines, T_r is the time constant of the wind turbines action, T_h is the turbine reheat time constant, F_H is the turbine high-pressure boiler duty cycle, ΔP_e is the electromagnetic power perturbation, ΔP_m is mechanical power variations, Δf is the frequency deviation, R_g is the modulation factor.

Neglecting the action delay of the wind turbine, that is, T_r is 0. The primary frequency modulation model shown in Fig. 1 has a transfer function as Eq. (3).

$$\begin{cases} F(s) = \dfrac{R_g T_h s + R_g}{As^2 + Bs + D_{equ} R_g + 1} \\ A = 2R_g H_{equ} T_h \\ B = 2H_{equ} R_g + R_g T_h D_{equ} + F_H T \end{cases} . \tag{3}$$

Among them,

$$\begin{cases} H_{equ} = H_{sys} + H_{RES} \\ D_{equ} = D_{sys} + D_{RES} \end{cases} . \tag{4}$$

For Eq. (3) shown, the expression of the time-domain response under the step perturbation is given by:

$$\Delta f(t) = \frac{R_g \Delta P_e}{1 + R_g D_{equ}} \left[1 + \alpha e^{-\omega_n \zeta t} \sin(\omega_r t + \phi)\right]. \tag{5}$$

Among them,

$$\begin{cases} \omega_n = \sqrt{\dfrac{R_g^{-1} + D_{equ}}{2T_h H_{equ}}}, \omega_r = \sqrt{\omega_n{}^2 (1 - \zeta^2)} \\ \alpha^2 (1 - \zeta^2) = 1 + F_H T_h \zeta \omega_n + T_h^2 \omega_n^2 \\ \zeta = \omega_n \dfrac{R_g^{-1} F_H T_h + 2H_{equ} + T_h D_{equ}}{2\left(R_g^{-1} + D_{equ}\right)} \end{cases}. \tag{6}$$

The time and value of the frequency deviation peaks are:

$$\begin{cases} t_{nadir} = \dfrac{1}{\omega_r} \arctan\left(\dfrac{T_h \omega_r}{T_h \omega_n \zeta - 1}\right) \\ \Delta f_{nadir} = \dfrac{R_g \Delta P_e}{1 + D_{equ} R_g} \left(1 + \sqrt{1 - \zeta^2} \alpha e^{-\omega_n \zeta t_{nadir}}\right) \end{cases}, \tag{7}$$

where t_{nadir} and Δf_{nadir} denote the time and value at which the frequency deviation peaks, respectively.

The maximum frequency deviation is an important indicator of frequency stability. In the following, the effect of short-time power shortage on the frequency stability of the system is discussed according to the effect of control strategy and control parameters on the maximum frequency deviation.

3.2 The Impact of Short-Term Power Shortage on Maximum Frequency Deviation

3.2.1 The Impact of Control Strategies on the Maximum Frequency Deviation

To investigate the impact of SPRT on maximum frequency deviation, the parameters for the system model shown in Fig. 3 are selected as shown in Table 2.

Table 2: Frequency stability control key elements analysis and calculation parameters

Parameter	Value
Total capacity *S*/MVA	100
Inertia time constant H_{equ}/s	5
Damping coefficient D_{equ}/pu	1
Proportion of wind-solar power generation units/%	40
Reheat time constant T_h/s	1
Electromagnetic power disturbance ΔP_e/pu	0.1

First, assume that the power curve of the renewable energy unit LVRT or DC commutation failure process is shown in the Fig. 4. In Fig. 4, the initial power of the power supply is P_0, after the occurrence of the LVRT, the power drops to P_{sag} for a duration of t_{LVRT}, after which it immediately recovers. Under the

above assumptions, the lowest frequency of the system occurs at time t_{LVRT}, and, according to Eq. (5) the expression for the minimum frequency is:

$$\Delta f_{\mathrm{nadir}} = \frac{R_{\mathrm{g}}\left(P_0 - P_{\mathrm{sag}}\right)}{1 + R_{\mathrm{g}} D_{\mathrm{equ}}}\left[1 + \alpha e^{-\omega_{\mathrm{n}}\zeta t_{\mathrm{LVRT}}} \sin\left(\omega_{\mathrm{r}} t_{\mathrm{LVRT}} + \phi\right)\right]. \tag{8}$$

If the governor's role is not considered, the energy deficiency brought by the short-time active power shortage will be borne entirely by the rotor kinetic energy. To simplify the theoretical analysis, the following assumptions are made first:

(i) During the power shortage period and the recovery process, the wind turbine or DC active power is as shown in Fig. 4;

(ii) The duration from power shortage to recovery is short, and the synchronous machine's speed control system is too late to act;

(iii) Ignore losses and load changes due to speed changes. When the system frequency changes, the load indeed responds to the frequency variation. For static loads, during the inertia response stage, the frequency deviation is extremely small. As a result, the change in static loads can be neglected. Regarding dynamic loads such as those from induction motors, according to the literature [20], induction motors do not affect the maximum ROCOF. In other words, induction motors have almost no impact on the inertia response stage.

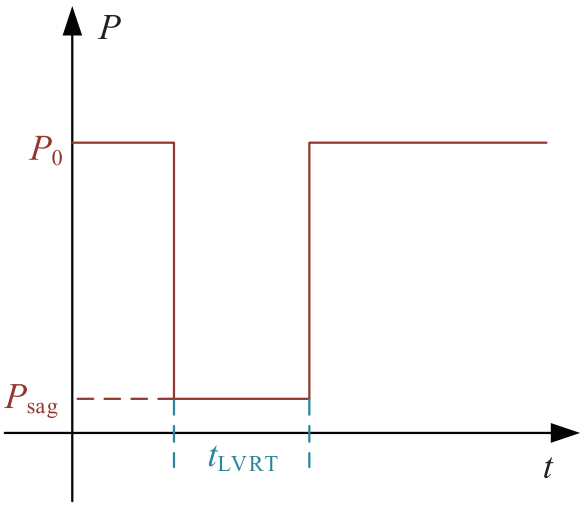

Figure 4: Simplified renewable energy units LVRT or DC commutation failure power curve

Under the above assumptions, the energy deficiency due to the SPRT will be fully balanced by the rotor kinetic energy of the synchronous machine. The energy deficiency due to short-time active power shortage can be summarized by Eq. (9) to calculate.

$$E_{\mathrm{LVRT}} = \int_0^{t_{\mathrm{LVRT}}} \left(P_0 - P_{\mathrm{sag}}\right) dt, \tag{9}$$

where E_{LVRT} is the energy deficiency due to SPRT. For a synchronous machine, the rotor kinetic energy released is:

$$E_{\mathrm{k}} = H_{\mathrm{equ}}\left(\omega_0^2 - \omega_f^2\right), \tag{10}$$

where E_k is the energy released from the kinetic energy of the synchronous machine rotor, ω_0 is the rated rotational speed, and ω_f is the rotational speed of the synchronous machine rotor after the failure. Under the preceding assumptions, the relation is satisfied:

$$E_k = E_{LVRT}. \tag{11}$$

Considering the effect of the governor, the expression for the lowest frequency of the system is given by Eq. (7). If the effect of the governor is not considered, the minimum frequency due to short-time active power shortage can be utilized in Eq. (8).

Taking the low-frequency penetration of renewable energy as an example, first assume that the duration of the low-frequency penetration is 300 ms. The minimum frequency of the system before and after considering the governor is shown in the Fig. 5. It can be seen that whether or not the governor is considered has a minimal impact on the calculation of the minimum frequency, with the maximum error not exceeding 2%.

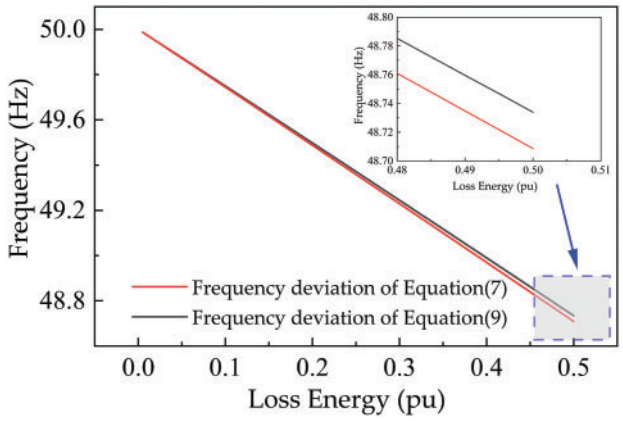

Figure 5: Calculated results of the lowest frequency of the system before and after considering the governor for wind turbines LVRT duration of 300 ms

Through the above analysis, it can be concluded that during the frequency variation caused by renewable energy low-frequency penetration, the governor has a minimal effect. The reason is that the governor's action time constant is relatively large, and within the time scale of renewable energy LVRT and recovery, the governor has a small impact on the change of mechanical power.

3.2.2 The Impact of LVRT Strategy Parameters on the Maximum Frequency Deviation

Under the system parameters shown in Table 2, the impact of LVRT parameters on system frequency stability is analyzed. Different proportions of wind and solar power generation are considered, with the system voltage maintained below 0.9 pu for a duration of 0.3 s, and the active power recovery time for wind and solar units from 0 to rated value set to 0.2 s. The system frequency variations resulting from LVRT of wind and solar units at different generation shares are shown in Fig. 6a.

By varying the amount of energy loss, the relationship between frequency deviation and energy loss is shown in Fig. 6b. According to Eq. (9), the system frequency deviation exhibits a square root relationship with energy loss. However, as observed in Fig. 6b, a nearly linear relationship exists between the two near the rated point. Therefore, the improvement in system frequency stability is almost proportional to the reduction

in energy loss during STPS. In high-renewable penetration power systems, adjusting the LVRT parameters of wind and solar units to minimize energy loss during LVRT periods plays a crucial role in enhancing system frequency stability.

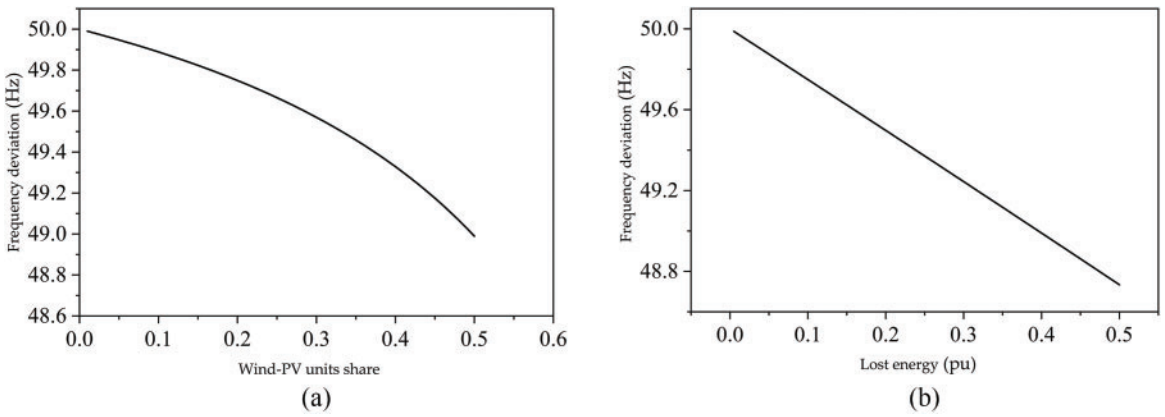

Figure 6: The impact of wind-PV on frequency. **(a)** The curve of frequency deviation caused by LVRT as a function of the wind and solar generation share; **(b)** The curve of frequency deviation caused by LVRT as a function of energy loss

From the above analysis process, it can be basically determined that the frequency instability of STPS brought about by renewable energy LVRT and DC commutation failure have the following characteristics:

(i) The frequency problem occurs on the power angle swing time scale, different units in the power system cannot be treated as the same frequency.

(ii) The energy deficiency is mainly compensated by the rotor kinetic energy of the units nearby, and the loss of rotor kinetic energy will be compensated back by the governor action in the following time.

(iii) The main cause of the frequency problem caused by the short-time active power shortage is not the shortage of the unit's frequency modulation capability but the magnitude and distribution of the unit's inertia. The closer the electrical distance and the larger the unit inertia, the more the speed of the unit is affected.

(iv) The frequency problem has regional characteristics. Evaluating the frequency problems brought about by LVRT of renewable units or DC commutation failures is essentially an evaluation of the system inertia magnitude and distribution.

4 Frequency Evaluation Method Based on Short-Time Active Power Shortage

Based on the conclusions of Section 3, to evaluate the ability to resist STPS of power system, this article proposes the concept of energy deficiency factor. The calculation formula for the energy deficiency factor is as follows:

$$K_{\mathrm{los}} = \frac{E_{\mathrm{los}}}{\alpha H_{\mathrm{equ}} \omega_0^2}, \tag{12}$$

where K_{los} denotes the energy deficiency factor, E_{los} denotes the energy deficiency brought about by the renewable energy units LVRT and DC commutation failure, ω_0 is the rated frequency, α is the maximum ratio of allowable energy loss, and it is taken as 1.

The energy deficiency factor is calculated as follows:

(i) Firstly, the system is partitioned according to inertia in a way that is based on the ability to maintain synchronization between different units under disturbance. In reality, the partitioning is generally done according to the geographical area.

(ii) For a given area, calculate the equivalent inertia for that area based on the inertia of each unit inside;

(iii) Assuming that there is a severe fault resulting in all renewable energy sources in the region with LVRT and all DC systems having commutation failure, or multiplying the total power of renewable energy sources and DC active power in the region by a low-voltage-ride-through ratio. The renewable energy loss during LVRT is determined by the percentage of active current of the renewable energy unit control parameter of LVRT, while the DC commutation failure is a total loss of power. The STPS can be calculated using the following equation.

$$P_{\mathrm{los}} = \left(1 - \alpha_{\mathrm{ap}}\right) P_{\mathrm{LVRT}} + P_{\mathrm{dc}}, \tag{13}$$

where P_{los} is the lost power of LVRT, α_{ap} is the percentage of active current of the renewable energy unit control parameter of LVRT, and P_{dc} is the total power of DC in the region.

(iv) The duration of LVRT is given by the simulation for a conservative period, taking the longest duration of renewable energy unit LVRT or DC commutation failure in all faults t_{max}, then the energy deficiency brought by renewable energy unit LVRT is defined as follows:

$$E_{\mathrm{los}} = \left[\left(1 - \alpha_{\mathrm{ap}}\right) P_{\mathrm{LVRT}} + P_{\mathrm{dc}}\right] t_{\mathrm{max}}. \tag{14}$$

The energy deficiency factor proposed in this paper aims to evaluate the spatial distribution of inertia. During the inertial response process in power systems, the entire grid indeed participates in the response. However, due to the existence of electrical distance, inter-regional power support capability weakens with increasing electrical distance, and fault propagation to remote areas also requires a longer time. Therefore, the calculation of the energy deficiency factor is conducted by region. For different regions in the system, there exists an energy deficiency factor, and the values of the energy deficiency factor are different for different regions.

5 Case Study

In order to verify the correctness of the theoretical analysis and the effectiveness of the energy loss factor, this paper conducts the case study of the East China Power Grid under three different operating conditions. For the East China Power Grid, inertia time constant and energy deficiency factors are calculated by province, with each province having an independent inertia time constant and energy deficiency factor. Firstly, inertia time constants H_{equ} are calculated. The inertia time constants are H_{equ}, as shown in Table 3. The calculation method and principle are in Eq. (4) and Fig. 3. Secondly, the energy loss factor is calculated and then verified through transient simulation. The results are shown in Table 4.

From the above Table 4, it can be seen that the energy deficiency factor of Jiangsu is the largest, while the energy deficiency factors of Anhui and Zhejiang are similar, and the energy deficiency factor of Fujian is the smallest. The reason is that the proportion of DC feed-in power and renewable energy in Jiangsu province is the largest, and the thermal power units in the province are relatively weak in resisting the energy deficiency caused by the LVRT of renewable energy and the failure of DC phase change.

Table 3: Inertia time constants H_{equ}/s under different operating conditions

Renewable energ penetration	Operating conditions		
Province	**Summer (20.2%)**	**Winter (35.6%)**	**High-proportion of renewable energy (42.2%)**
Fujian	4.37	4.44	4.40
Jiangsu	4.95	5.04	5.05
Anhui	4.41	4.53	4.71
Zhejiang	4.51	4.53	4.55

Table 4: Energy deficiency factors in different regions

Renewable energy penetration	Operating conditions		
Province	**Summer (20.2%)**	**Winter (35.6%)**	**High-proportion of renewable energy (42.2%)**
Fujian	0.11	0.15	0.11
Jiangsu	0.40	0.40	0.37
Anhui	0.20	0.19	0.17
Zhejiang	0.15	0.19	0.17

5.1 Renewable Energy Units LVRT

Select a renewable energy station in Zhejiang Province in the East China Power Grid under high-proportion of renewable energy operating condition. Apply a three-phase short circuit fault at the 230 kV bus where the renewable energy station is connected to a power grid, causing renewable energy units to enter the LVRT and block active power output. During the short-circuit fault, the output of the renewable energy unit is completely unable to be sent out, and after the fault is cleared, renewable energy units still maintain a short-term LVRT state, which lasted for nearly 100 ms before recovery. The changes in unit speed in various provinces due to the STPS of renewable energy are shown in Fig. 7.

As can be seen from the above waveforms, except for Zhejiang, the speed change of units in other provinces changes very little. Thus, it shows that the short-time active power shortage in Zhejiang province caused by renewable energy units LVRT is mainly compensated by the rotor kinetic energy of the units in Zhejiang province, and the loss of rotor kinetic energy will be compensated back by the governor action in the following time. Even in the Zhejiang province, the rotational speeds of different units are different, and there is almost no moment of the same frequency in the whole transient process. This also corroborates the conclusion discussed above, that is, the impact of short-time active power shortage caused by the renewable energy units LVRT occurs in the power angle swing phase.

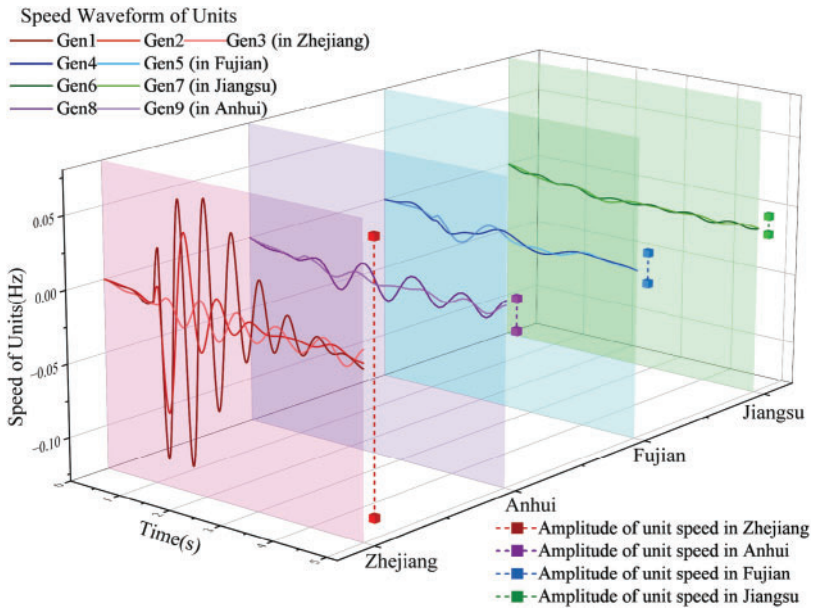

Figure 7: Speed waveform of typical units in different provinces caused by renewable unit LVRT

5.2 DC Commutation Failure

In the East China Power Grid, under the high proportion of renewable energy operation, the 525 kV inverter bus Mudu of Baihetan-Jiangsu DC system in Jiangsu Province is selected. Apply a three-phase short circuit fault at the Mudu bus of the inverter, and after the fault lasts for 100 ms, cut it off and disconnect one of the Mudu bus's outgoing lines (N-1 fault). After the fault is cleared, the DC system unit still maintains commutation failure, which lasted for nearly 400 ms before DC power started to recover. The changes in unit speed in various provinces due to the STPS of DC commutation failure are shown in Fig. 8.

From Fig. 8, it can be seen that the units in Jiangsu Province have been greatly affected, mainly due to long-term commutation failure of the Baihetan-Jiangsu DC system. Among all typical units, the speed change amplitude of Gen6 in Jiangsu Province is the largest, with the lowest speed approaching 49.6 Hz. This verifies that the frequency variation caused by STPS is related to the inertia distribution of the system, and the energy deficiency factor also has a good indicative significance. Except for Jiangsu, the speed variation of units in other provinces is very small. This indicates that the STPS caused by DC commutation failure in Jiangsu Province is mainly compensated for by the rotor kinetic energy of the units in Jiangsu Province. This also corroborates the conclusion discussed above, that is, the impact of short-time active power shortage caused by the DC commutation failure occurs in the power angle swing phase.

From Fig. 8, it can be seen that the units in Jiangsu Province have been greatly affected, mainly due to long-term commutation failure of the Baihetan-Jiangsu DC system. Among all typical units, the speed change amplitude of Gen6 in Jiangsu Province is the largest, with the lowest speed approaching 49.6 Hz. This verifies that the frequency variation caused by STPS is related to the inertia distribution of the system, and the energy deficiency factor also has a good indicative significance. Except for Jiangsu, the speed variation of units in other provinces is very small. This indicates that the STPS caused by DC commutation failure in Jiangsu Province is mainly compensated for by the rotor kinetic energy of the units in Jiangsu Province. This also corroborates the conclusion discussed above, that is, the impact of short-time active power shortage caused by the DC commutation failure occurs in the power angle swing phase.

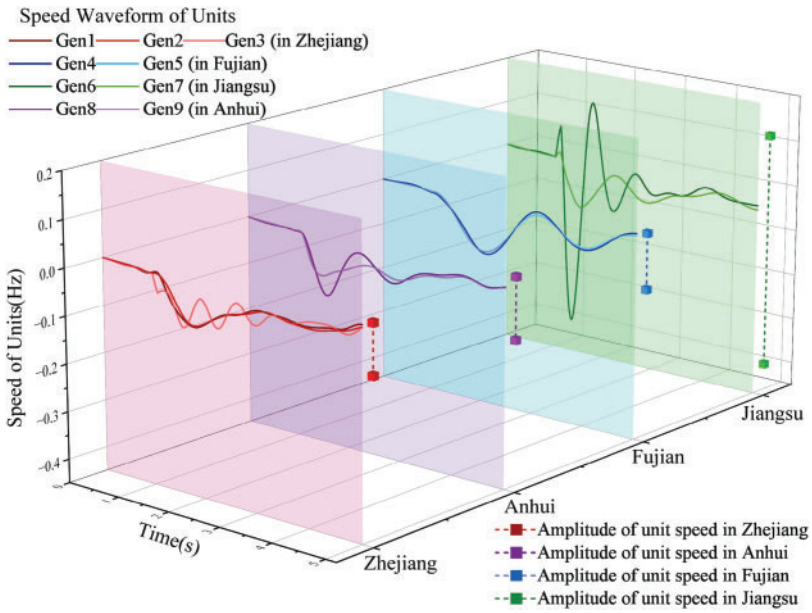

Figure 8: Speed waveform of typical units in different provinces caused by DC commutation failure

5.3 Multi-DC Commutation Failure

In addition, considering a fault with a larger affected area, a high proportion of renewable energy operating conditions were selected. A three-phase metallic short circuit fault was applied to the 1050 kV bus in Anji, Zhejiang Province. After the fault lasted for 100 ms, it was cut off, and one of the Anji 1050 kV Lanjiang 1050 kV double circuit lines was tripped. The speed changes of some units in each province are as follows.

From Fig. 9, it can be seen that the units in Zhejiang Province have been greatly affected, mainly due to the short-circuit fault at Anji Lanjiang, which caused commutation failures of multiple DC lines, including Baihetan Zhejiang DC, Lingshao DC, and Binjin DC. In particular, the Baihetan Zhejiang DC failed to recover after a long period of commutation failure, and it took nearly 200 ms for the short-circuit fault to be cleared before normal recovery; At the same time, it also caused renewable energy stations such as Zhejiang Anjiang and Zhejiang Changlong to enter the underpass, resulting in a short-term shortage of renewable energy power. Among them, the speed fluctuation of the Zhejiang Changlong unit is the largest, with the lowest speed approaching 49.5 Hz.

From Fig. 9, it can be seen that compared to the units in Zhejiang province, the speed changes of units in other provinces are relatively small. This indicates that the STPS caused by the Anji Lanjiang N-1 fault is mainly compensated for by the rotor kinetic energy of the units in Zhejiang Province, and the lost rotor kinetic energy will be compensated for later by the action of the governor. This once again confirms the conclusion drawn earlier, that is, the impact of STPS caused by low penetration or DC commutation failure of renewable energy occurs during the power angle swing stage. However, compared to the fault conditions of Zhejiang Taihan, the speed changes of other units in other provinces under the Anji Lanjiang N-1 fault are relatively large. This is because the Anji Lanjiang N-1 fault is electrically connected through the ultra-high voltage line, causing other STPS in the province. For example, in Jiangsu province, due to the impact of the Anji Lanjiang N-1 fault, there was a commutation failure in both the Fu Feng DC and Jin Su DC, which led to the entry of renewable energy sources, such as Su Xufeng and Su Wuqiao into the underpass, resulting

in a STPS. As a result, the speed changes of units in Jiangsu province under this fault are larger than those under the Zhejiang Taihan fault.

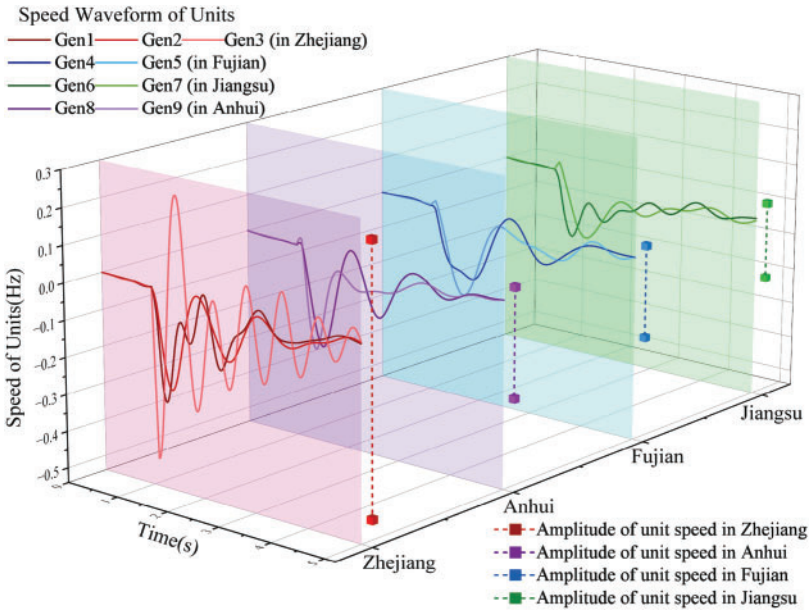

Figure 9: Speed waveform of typical units in different provinces caused by multi-DC commutation failure

6 Conclusion

To address the frequency instability by LVRT of renewable energy units and DC commutation, this paper firstly establishes the frequency response model, and analyses the mechanism of frequency instability caused by STPS, and proposes the index of the energy deficiency factor to evaluate the impact of the short-time power shortage on the frequency stability of the region. The main conclusions are as follows:

(i) The frequency instability of STPS caused by LVRT of renewable energy units and DC commutation occurs on the power angle swing time scale, different units in the power system cannot be treated as the same frequency.

(ii) The energy deficiency is mainly compensated by the rotor kinetic energy of the units nearby, and the loss of rotor kinetic energy will be compensated back by the governor action in the following time. So the main cause of the frequency problem caused by the STPS is not the shortage of the unit's frequency modulation capability, but the magnitude and distribution of the unit's inertia, which means this frequency problem has a regional characteristic.

(iii) This paper adopts the concept of energy deficiency factor to evaluate the impact of the STPS on the frequency of the region. This paper selects the East China Power Grid as the test system. The result verifies the proposed mechanism of STPS on the frequency of the novel power system at the receiving end and shows that the energy deficiency factor has certain guiding significance.

The energy deficiency factor proposed in this paper can be used to evaluate frequency stability issues caused by STPS. However, there are still some limitations in the text, such as simplifications made during the analysis, including neglecting the impact of load and not addressing how to use the energy deficiency factor to improve the system's frequency stability.

Future work could focus on expanding the analysis to larger power grids with higher renewable energy penetration to validate the proposed energy deficiency factor. Additionally, integrating advanced control strategies like demand response and energy storage could mitigate the impact of STPS on system frequency. Investigating region-specific control mechanisms and exploring hybrid AC/DC systems with renewable sources could improve grid resilience. Lastly, real-time application of the energy deficiency factor could lead to decision-making tools for grid operators, enhancing operational efficiency and stability.

Acknowledgement: Not applicable.

Funding Statement: This research was funded by the Technology Project of State Grid Corporation of China (Research on Safety and Stability Evaluation and Optimization Enhancement Technology of Flexible Ultra High Voltage Multi-terminal DC System Adapting to the Background of "Sand and Gobi Deserts"), grant number J2024003.

Author Contributions: The authors confirm contribution to the paper as follows: writing—original draft preparation, Wenjia Zhang; writing—review and editing, Sixuan Xu, Wanchun Qi, Zhuyi Peng, and Wentao Sun. All authors reviewed the results and approved the final version of the manuscript.

Availability of Data and Materials: The authors confirm that the data supporting the findings of this study are available within the article.

Ethics Approval: Not applicable.

Conflicts of Interest: The authors declare no conflicts of interest to report regarding the present study.

Nomenclature

LVRT	Low voltage ride through
LCC-HVDC	Line commutated converter high voltage direct current
STPS	Short-term power shortage
ROCOF	Rate of change of frequency
t_{nadir}	The time of the frequency deviation peaks
$\Delta f_{\mathrm{nadir}}$	The value of the frequency deviation peaks
H_{equ}	Equivalent inertia
K_{los}	The energy deficiency factor
E_{los}	The energy deficiency brought about by the renewable energy units LVRT and DC commutation failure
ω_0	The rated frequency

References

1. Ratnam KS, Palanisamy K, Yang G. Future low-inertia power systems: requirements, issues, and solutions—a review. Renew Sustain Energy Rev. 2020;124:109773. doi:10.1016/j.rser.2020.109773.
2. Zhang K, Cui Y, Yang Z, Feng Y, Zhang Q, Yu Y. Analysis of the influence of synchronous condensers on receiving-end grid with multiinfeed HVDC. In: Proceedings of the 2016 IEEE International Conference on Power System Technology (POWERCON); 2016 Sep 28–Oct 1; Wollongong, NSW, Australia. p. 1–6. doi:10.1109/POWERCON.2016.7753867.
3. Kabsha MM, Moursi MS, El-Fouly TH, Al-Durra A. Frequency and voltage disturbances ride-through control strategy for PV power plants. IEEE Trans Sustain Energy. 2025;16(2):1068–83. doi:10.1109/TSTE.2024.3497975.
4. Acosta JS, Xiao H, Gole AM. Sensitivity analysis of commutation failure in multi-infeed HVDC systems: exploring the impact of ac system representations and fault types. Electr Power Syst Res. 2024;234:110802. doi:10.1016/j.epsr.2024.110802.
5. Liu L, Li W, Ba Y, Shen J, Jin C, Wen K. An analytical model for frequency nadir prediction following a major disturbance. IEEE Trans Power Syst. 2020;35(4):2527–36. doi:10.1109/TPWRS.2019.2963706.

6. Egido I, Fernandez-Bernal F, Centeno P, Rouco L. Maximum frequency deviation calculation in small isolated power systems. IEEE Trans Power Syst. 2009;24(4):1731–8. doi:10.1109/TPWRS.2009.2030399.
7. O' Sullivan J, Rogers A, Flynn D, Smith P, Mullane A, O' Malley M. Studying the maximum instantaneous non-synchronous generation in an island system—frequency stability challenges in Ireland. IEEE Trans Power Syst. 2014;29(6):2943–51. doi:10.1109/TPWRS.2014.2316974.
8. Wang Y, Strbac G. Transient stability-driven planning for the optimal sizing of resilient AC/DC hybrid microgrids. IEEE Trans Power Syst. 2025;40(3):2777–90. doi:10.1109/TPWRS.2024.3505142.
9. Yan SR, Dai Y, Shakibjoo AD, Zhu L, Taghizadeh S, Ghaderpour E, et al. A fractional-order multiple-model type-2 fuzzy control for interconnected power systems incorporating renewable energies and demand response. Energy Rep. 2024;12:187–96. doi:10.1016/j.egyr.2024.06.018.
10. Dai J, Tang Y, Wang Q, Jiang P, Hou Y. An extended SFR model with high penetration wind power considering operating regions and wind speed disturbance. IEEE Access. 2019;7:103416–26. doi:10.1109/ACCESS.2019.2930807.
11. Qazi HW, Wall P, Val Escudero M, Carville C, Cunniffe N, O'Sullivan J, et al. Impacts of fault ride through behavior of wind farms on a low inertia system. IEEE Trans Power Syst. 2022;37(4):3190–8. doi:10.1109/TPWRS.2020.3003470.
12. Njoka GM, Mogaka L, Wangai A. Impact of variable renewable energy sources on the power system frequency stability and system inertia. Energy Rep. 2024;12:4983–97. doi:10.1016/j.egyr.2024.10.057.
13. Pei J, Yao J, Liu R, Zeng D, Sun P, Zhang H, et al. Characteristic analysis and risk assessment for voltage-frequency coupled transient instability of large-scale grid-connected renewable energy plants during LVRT. IEEE Trans Ind Electron. 2020;67(7):5515–30. doi:10.1109/TIE.2019.2931256.
14. Choopani M, Hosseinian SH, Vahidi B. New transient stability and LVRT improvement of multi-VSG grids using the frequency of the center of inertia. IEEE Trans Power Syst. 2020;35(1):527–38. doi:10.1109/TPWRS.2019.2928319.
15. Rahimi E, Gole AM, Davies JB, Fernando KL, Kent KL. Commutation failure analysis in multi-Infeed HVDC systems. IEEE Trans Power Deliv. 2011;26(1):378–84. doi:10.1109/TPWRD.2010.2081692.
16. GB/T 19963.1-2021. Technical specification for connecting wind farm to power system. Part 1: on shore wind power. Beijing, China: Standards Press of China. 2021 [cited 2025 Feb 07]. Available from: https://openstd.samr.gov.cn/bzgk/std/newGbInfo?hcno=F0127C2B431AC283CD6ED17CE67F8E46.
17. Shu H, Wang G, Chen J, Ma H, He T. Coordinated control of wind-storage combined with primary frequency regulation and variable coefficient based on wind speed and SOC. J Energy Storage. 2024;87:111356. doi:10.1016/j.est.2024.111356.
18. Chan ML, Dunlop RD, Schweppe F. Dynamic equivalents for average system frequency behavior following major distribances. IEEE Trans Power Appar Syst. 1972;PAS-91(4):1637–42. doi:10.1109/TPAS.1972.293340.
19. Shen J, Li W, Liu L, Jin C, Wen K, Wang X. Frequency response model and its closed-form solution of two-machine equivalent power system. IEEE Trans Power Syst. 2021;36(3):2162–73. doi:10.1109/TPWRS.2020.3037695.
20. Chen L, Wang X, Min Y, Li G, Wang L, Qi J, et al. Modelling and investigating the impact of asynchronous inertia of induction motor on power system frequency response. Int J Electr Power Energy Syst. 2020;117:105708. doi:10.1016/j.ijepes.2019.105708.